applied sciences

MDPI

Article

# Quantitative Evaluation of Food-Waste Components in Organic Fertilizer Using Visible–Near-Infrared Hyperspectral Imaging

**Geonwoo Kim [1,2], Hoonsoo Lee [3,*], Byoung-Kwan Cho [4], Insuck Baek [2,5] and Moon S. Kim [2]**

[1] Department of Bio-Industrial Machinery Engineering, College of Agriculture and Life Science, Gyeongsang National University, Jinju 52828, Korea; geonwookim@gnu.ac.kr
[2] Environmental Microbial and Food Safety Laboratory, Agricultural Research Service, United States Department of Agriculture, Powder Mill Rd, Building 303, BARC-East, Beltsville, MD 20705, USA; insuck.baek@usda.gov (I.B.); moon.kim@usda.gov (M.S.K.)
[3] Department of Biosystems Engineering, College of Agriculture, Life & Environment Science, Chungbuk National University, Chungdae-ro, Seowon-gu, Cheongju 28644, Korea
[4] Department of Biosystems Machinery Engineering, College of Agricultural and Life Science, Chungnam National University, 99 Daehak-ro, Yuseoung-gu, Daejeon 34134, Korea; chobk@cnu.ac.kr
[5] Oak Ridge Institute for Science and Education, 1299 Bethel Valley Rd, Oak Ridge, TN 37830, USA
* Correspondence: hslee202@chungbuk.ac.kr

**Abstract:** Excessive addition of food waste fertilizer to organic fertilizer (OF) is forbidden in the Republic of Korea because of high sodium chloride and capsaicin concentrations in Korean food. Thus, rapid and nondestructive evaluation techniques are required. The objective of this study is to quantitatively evaluate food-waste components (FWCs) using hyperspectral imaging (HSI) in the visible–near-infrared (Vis/NIR) region. A HSI system for evaluating fertilizer components and prediction algorithms based on partial least squares (PLS) analysis and least squares support vector machines (LS-SVM) are developed. PLS and LS-SVM preprocessing methods are employed and compared to select the optimal of two chemometrics methods. Finally, distribution maps visualized using the LS-SVM model are created to interpret the dynamic changes in the OF FWCs with increasing FWC concentration. The developed model quantitatively evaluates the OF FWCs with a coefficient of determination of 0.83 between the predicted and actual values. The developed Vis/NIR HIS system and optimized model exhibit high potential for OF FWC discrimination and quantitative evaluation.

**Keywords:** organic fertilizer; food waste; hyperspectral imaging; partial least squares; support vector machine

check for updates

**Citation:** Kim, G.; Lee, H.; Cho, B.-K.; Baek, I.; Kim, M.S. Quantitative Evaluation of Food-Waste Components in Organic Fertilizer Using Visible–Near-Infrared Hyperspectral Imaging. *Appl. Sci.* **2021**, *11*, 8201. https://doi.org/10.3390/app11178201

Academic Editor: Dick Sterenborg

Received: 8 July 2021
Accepted: 1 September 2021
Published: 3 September 2021

**Publisher's Note:** MDPI stays neutral with regard to jurisdictional claims in published maps and institutional affiliations.

**Copyright:** © 2021 by the authors. Licensee MDPI, Basel, Switzerland. This article is an open access article distributed under the terms and conditions of the Creative Commons Attribution (CC BY) license (https://creativecommons.org/licenses/by/4.0/).

## 1. Introduction

With the increasing growth of the global economy and population, the associated increase in food consumption has resulted in large volumes of food waste (FW). Moreover, the amount of FW is predicted to grow by 44% from 2005 to 2025 [1]. FW is usually incinerated with municipal solid waste or dumped in landfills [2,3]. However, incineration and landfills can have harmful effects on human health and can contribute to global warming and environmental pollution through toxic gas emission, ground water contamination, air pollution, fire hazards, and so on [2,4,5]. Thus, FW should be properly managed to prevent negative environmental impact. Therefore, recycling technology and related biotechnology are undergoing rapid development [2,6–8].

As a typical recycling method, FW is often converted into organic fertilizer (OF) because the former is a valuable resource that contains plant nutrients, which can mitigate the serious organic matter deficit of agricultural soils [2,3]. Despite the advantages of FW fertilizer, in the Republic of Korea, it is not considered a good additive for OF because of its high level of sodium chloride (NaCl). Note that soil salinity is one of the most significant abiotic constraints, as high salinity severely affects agricultural productivity and disturbs the soil nutrition balance [9]. The high NaCl concentrations in Korean food are attributed to kimchi, soy sauce, and soybean paste, which are fermented and stored in high-saline water for food preservation. Therefore, NaCl is a limiting factor for FW fertilizer production with Korean FW [10]. In addition, kimchi has high capsaicin content, and capsaicin has negative effects on plant growth; this is another major limiting factor for FW fertilizer [11]. Thus, the government of the Republic of Korea has restricted the NaCl content in OF to 2% and established the maximum permissible content of Korean FW in OF as 30% [12]. However, some entrepreneurs have recently produced OF mixed with a high percentage of Korean FW (over 30%) to reduce production costs. These illegal products have been distributed and sold nationwide. Therefore, a nondestructive evaluation technique for food-waste components (FWC) in OF has drawn considerable research attention.

Hyperspectral imaging (HIS) can simultaneously acquire spatial and spectral data from a target by combining image processing and spectroscopy techniques, and is a powerful tool for agricultural analyses [13–15]. Rapid improvements in HSI technology have facilitated nondestructive evaluation of soil nutrition, fertilizer quality, plant productivity, and so on. HSI technology has also been used in fertilizer nutrient analysis, salt stress assessment, plant growth monitoring according to fertilizer type, etc. For instance, An et al. (2016) developed a soil salinity model for satellite hyperspectral remote-sensing data and used it to evaluate salt stress on winter wheat [16]. Further, Kumar et al. (2018) investigated the spectral signature of a soil and fertilizer mixture and developed a quantification equation incorporating the diagnostic depth and the soil fertilizer concentration [17]. Wang et al. (2018) evaluated the nitrogen fertilizer levels of a tea plant using visible and near-infrared HSI techniques with multivariate classification algorithms; hence, they discriminated tea plants subjected to three different nitrogen treatments [18]. Finally, Sha et al. (2019) proposed a HSI method, including multivariate techniques, to discriminate fertilized from unfertilized grasses and showed that specific wavelengths can be effectively used to assess the influence of different fertilizers on the grasses [19]. However, to the best of the authors' knowledge, no nondestructive HIS technology for FWC evaluation in OF within the visible–near-infrared (Vis/NIR) region has been developed to date. Vis/NIR spectroscopy has been widely known to be one of the most effective techniques for visualization of soil nutrient contents and their related distributions, and for rapid evaluation of fertilizer components [20].

The primary aim of this study is to develop an optimal model for qualitatively and quantitatively detecting FWCs in OF, based on the Vis/NIR HIS technique. To accomplish this, the minor objectives are the following: (1) analysis of the spectroscopic data of OF and FW fertilizer raw materials, (2) calculation of the NaCl and capsaicin concentrations in FWC using inductively coupled plasma optical emission spectroscopy (ICP-OES), (3) development of optimal models for OF FWC evaluation, and (4) acquisition of hyperspectral images suitable for OF FWC detection based on pixel information using the developed optimal models. Partial least squares (PLS) and least-squares support vector machine (LS-SVM) techniques are used to develop the optimal model because these techniques have been widely used for nondestructive evaluation of biochemical and biophysical variables in various agricultural applications [18,21–24]. In addition, to improve the performance of the developed models, various pre-preprocessing methods are applied. Hence, the potential for qualitative and quantitative evaluation of OF FWCs is investigated using the developed optimal model based on HSI technology.

## 2. Materials and Methods

### 2.1. Sample Preparation

Raw materials of OF and commercial FW fertilizer (Daewon-Nongsan, Chungbuk, Republic of Korea) were purchased for NaCl concentration analysis and hyperspectral image acquisition. Six OF raw materials were selected: castor oil cake, rapeseed oil cake, soybean oil cake, bone dust, rice bran, and fish meal; these items are widely consumed in Korea. The spectral data of the six raw materials and FW fertilizer were then obtained. The FW fertilizer was uniformly mixed with the raw materials, for FWC concentrations ranging from 0 to 100%, i.e., 0, 5, 10, 15, 20, 30, 40, 50, and 100%, and the spectral data of the various samples within the Vis/NIR region were obtained. A total of 275 mixture samples with different FWC concentrations were fabricated on the laboratory scale. FW fertilizer and OF particle sizes were measured as ranging from 0.1 to 5 mm.

The ICP-OES method, one of the most widely used physicochemical analysis techniques in agricultural studies [25,26], was used to analyze the NaCl concentrations in the six major OF components and FW fertilizer. Table 1 lists the ICP-OES measurement results (ICP-OES 5100 series, Agilent Technologies, Santa Clara, CA, USA).

**Table 1.** NaCl concentrations of major materials used for organic fertilizer in Korea.

| Materials | NaCl (mg/g) | Capsaicin (mg/g) |
|---|---|---|
| FW fertilizer | 752.52 | 1637.31 |
| Castor oil cake | 57.29 | 0 |
| Rapeseed oil cake | 37.77 | 0 |
| Soybean oil cake | 2.56 | 0 |
| Bone dust | 479.32 | 0 |
| Rice bran | 9.64 | 0 |
| Fish meal | 412.58 | 0 |

In Table 1, FW fertilizer, bone dust, and fish meal have relatively high NaCl concentrations compared to the plant-based OF materials. Only the FW fertilizer has a very high level of capsaicin. As expected, although bone dust and fish meal have higher NaCl levels than the other components, the FW fertilizer has the highest concentrations of both NaCl and capsaicin.

### 2.2. Hyperspectral Imaging System

The line-scan-based HSI technique was used in this study as it allows rapid detection of the physical and chemical information of a sample in terms of the spectral data. These data are obtained for each spatial pixel of a captured image and a three-dimensional (3D) hyperspectral cube is simultaneously produced [27–29]. Figure 1 is a conceptual diagram of the Vis/NIR HSI system based on the line-scan method employed in this work.

The main components are a 400–1000-nm low-light sensitive electron-multiplying charge-coupled-device (EMCCD; MegaLuca, Andor Technology Inc., Belfast, Northern Ireland) camera including a detector array of 1002 vertical and 1004 horizontal pixels thermo-electrically cooled to $-20$ °C via a two-stage Peltier cooler; an imaging spectrograph (VNIR Hyperspec, Headwall Photonics Inc., Fitchburg, MA, USA) for line-scan imaging; a Schneider–Kreuznach Xenoplan 1.4/23 C-mount lens (Schneider Optics, Hauppauge, NY, USA); six 100-W quartz–tungsten halogen lamps.

Line-scan imaging was achieved when light from the line-scanned field of view (FOV) was passed through the slit of the imaging spectrograph. Here, to produce a 2D image featuring the spatial (horizontal axis) and spectral (vertical axis) dimensions, the light was dispersed and then projected by the dispersive gratings of the EMCCD detector array. The lamps were integrated with fiber-optic line lights (Fiber-Lite, Dolan-Jenner Industries Inc., Lawrence, MA, USA) positioned 500 mm from the sample and 220 mm apart to illuminate the line-scan FOV at forward and backward angles of approximately 10° with respect to the vertical. The samples were transported by a programmable motorized translation sample holder (25 mm $\times$ 25 mm $\times$ 3 mm; Velmex, Inc., Bloomfield, NY, USA) under illumination, and their hyperspectral line-scan images were taken using a 0.2-mm incremental step.

### 2.3. Hyperspectral Image Acquisition

The displacement of the sample translation unit was 210 mm in 0.2-mm increments under illumination (500 mm below the camera lens), and the single-pixel size of the hyperspectral image was 0.2 mm. The hyperspectral data of the mixture samples were acquired simultaneously during translation. The scan area described by one pixel was 0.04 mm$^2$

[0.2 mm (spatial) × 0.2 mm (scan)]. The camera region of interest (ROI) was identical to the translation unit size (25 mm × 25 mm). The backgrounds of the sample images were removed by setting the pixels to zero, to exclude unnecessary pixel information. Thus, the specifications of the obtained 3D hypercubes of each sample were 125 (spatial) × 125 (scan) pixels with 128 wavelengths (channels), excluding their backgrounds.

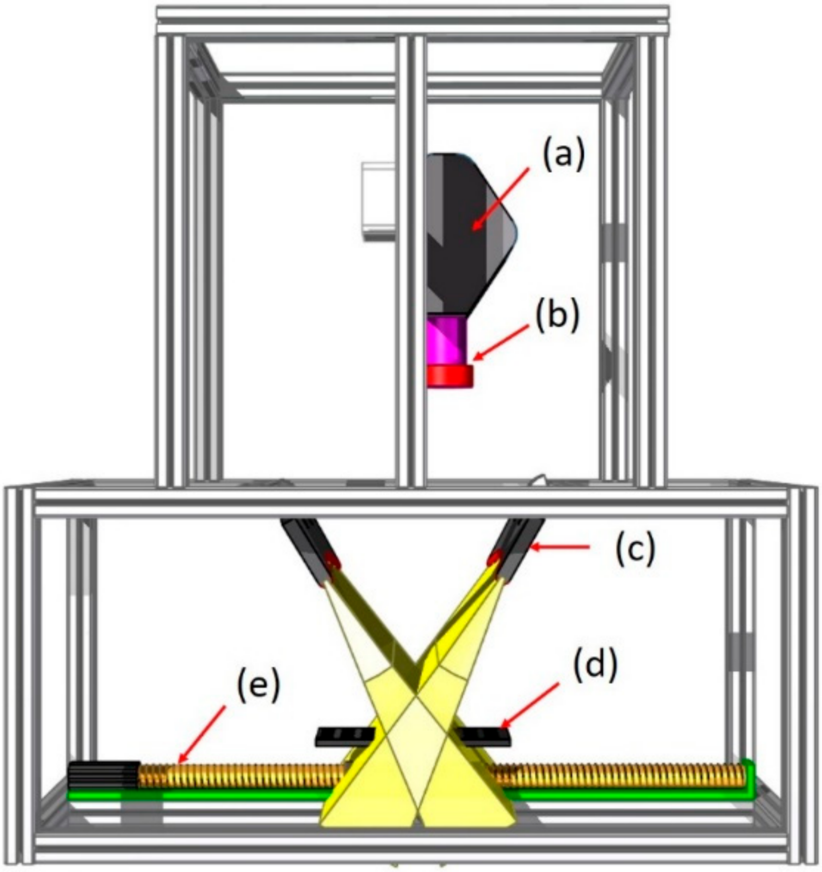


**Figure 1.** Conceptual diagram of HSI system: (**a**) imaging spectrograph with electron-multiplying CCD, (**b**) C-mount lens, (**c**) quartz–tungsten halogen lamps, (**d**) sample holder, and (**e**) programmable monoaxial stage.

The actual spectral information of the hyperspectral images was obtained through relative reflectance correction (spectral calibration) of the sample images, using a 99% diffuse reflectance white reference image (SRT-99-120, Labsphere, North Sutton, NH, USA) and a dark reference image. The dark reference image was acquired by deactivating the illumination and was obtained to enable correction for noise from the EMCCD camera. The spectral calibration reflectance values were acquired according to the following equation [14,30]:

$$I_R = \frac{I_r - I_b}{I_w - I_b} \tag{1}$$

where $I_R$ is the relative reflectance image and $I_r$, $I_w$, and $I_b$ are the obtained hyperspectral, white reference, and black reference images, respectively. Before image processing for FWC detection in the mixture samples, the spectral data of the raw materials were acquired for analysis of their chemical characteristics. Then, after background removal and spectral calibration, the hyperspectral images of the samples were used to develop the optimal model.

### 2.4. Model Delvelopment

PLS and SVM techniques were chosen for the main algorithms used to develop the FW-component detection models. PLS is a multivariate analysis method that extracts new latent variables or factors from raw spectra. These factors indicate the maximum covariance between the reference and spectral information [13]. Thus, the PLS method can resolve the multi-collinearity problem using the latent variables of the independent and dependent variables. Unlike the PLS technique, the LS-SVM method can optimize separation of hyperspectral matrixes that minimize the misclassification rate for groups and can solve non-linear problems [31,32]. By comparing the results of both techniques, the linear and non-linear features of the OF FW component evaluation could be compared and analyzed. Of the 275 samples, 205 and 70 were used for model development and prediction, respectively.

To enhance the forecasting capacity and robustness of calibration of the PLS and LS-SVM models, it is important to derive the effective wavelength (EW) region and PLS factors [33]. The EW regions were selected using the intermediate PLS (iPLS) method, which can prevent overlap and weak absorption intensity in the obtained spectral data. The effective PLS factors were determined from the minimum root mean square error of the validation (RMSEV) value and the EW regions were extracted using a baseline lower than the average RMSEV values. The RMSEV values were calculated from the following equation [33]:

$$\text{RMSEV} = \sqrt{\frac{\sum_{i=1}^{n}\left(y_{i,\ actual} - y_{i,\ predicted}\right)^2}{n}} \quad (2)$$

where $y_{i,actual}$ and $y_{i,predicted}$ are the actual and estimated values for the developed PLS model, respectively, and $n$ indicates the actual/predicted samples. To accomplish this, the total wavelength was divided by 50-nm intervals and the regions lower than the average of the entire subinterval were selected as the EW regions.

To improve the performance of both models, five spectral preprocessing methods were applied to the hyperspectral images of the samples: multiplicative scatter correction (MSC), standard normal variate (SNV) transformation, the Savitzky–Golay derivative (SGD), smoothing, and normalization methods. These processes simplified the obtained spectrum such that the spectral peaks (corresponding to specific chemical characteristics) were emphasized through removal of noise signals such as scattering effects generated by the irregular surfaces of the samples and irregular changes in the illumination paths and intensity [22,33]. Among them, a preprocessing method with a low standard error of calibration (SEC), a low standard error of prediction (SEP), and a high coefficient of determination ($R^2$) was selected to realize the optimal model imaging.

### 2.5. Image Processing

The HSI technique can create pixel images or a chemical concentration map based on the spatial distribution of the chemical components in the sample. In this study, the predicted hyperspectral images were determined based on the FWC quantity and allowed improved interpretation of the sample chemical dynamics and distribution patterns based on the contained pixel information. The obtained hyperspectral images were also processed by removing the backgrounds of the sample images and through application of preprocessing methods. The higher the peaks of the beta-coefficient absolute values in the PLS model, the greater the effect on the model development. Hyperspectral images for qualitative and quantitative evaluation of the OF FWCs were acquired using the above procedures and image processing technique. The workflow of the HSI data processing procedures is shown in Figure 2. All pixel mapping, data analysis, HSI control, model development, and image processing were implemented using Matlab software (version 7.13; MathWorks Inc., Natick, MA, USA) with a Microsoft Windows operating system (Windows 10; Microsoft, Redmond, WA, USA).

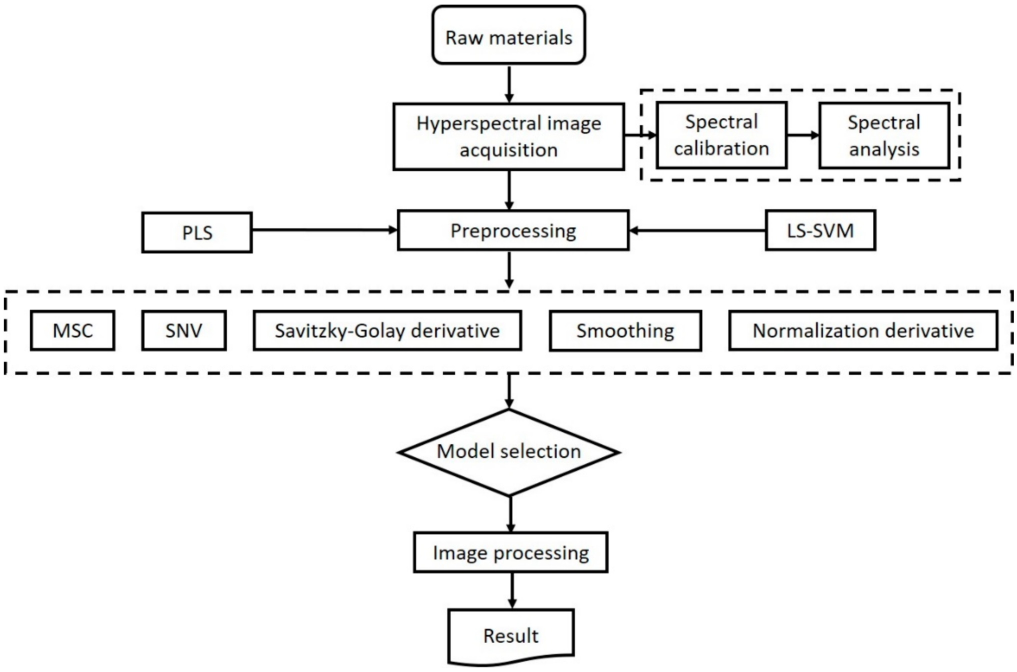


**Figure 2.** Workflow of HSI analysis for qualitative and quantitative evaluation of OF FW components.

## 3. Results

### *3.1. Spectral Data*

Figure 3 shows the spectral data obtained for the mixture samples and FW fertilizer within the Vis/NIR region using the HSI system. Figure 3a,b show the raw spectral data of the mixture samples for different FWC content ratios (0 to 100%) and their average values, respectively.

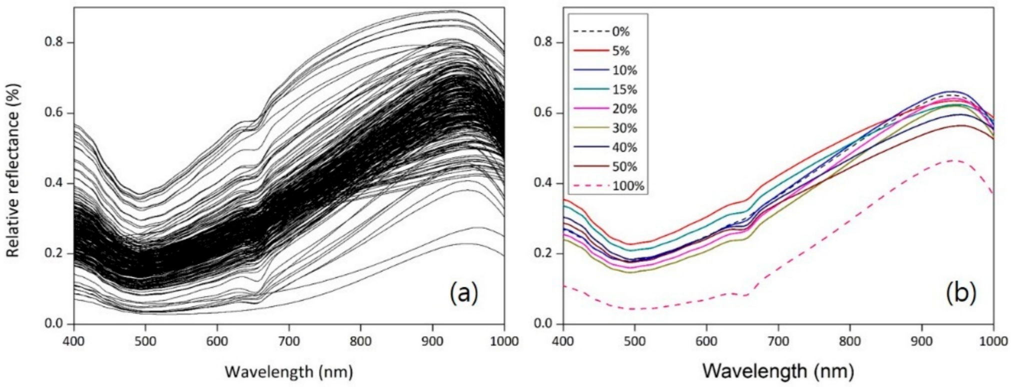


**Figure 3.** Spectral data of mixture samples with increasing FWC concentration (0, 5, 10, 15, 20, 30, 40, 50, and 100%): (**a**) whole and (**b**) average spectra.

### *3.2. Model Development*

As noted above, incorporation of all wavelengths also includes unrelated information for modeling and noise, which can cause multicollinearity and data overlap problems [27]. To avoid these issues and improve the FWC model predictability, EW regions were defined and applied to both PLS and LS-SVM models. These EW regions were selected using a baseline that was lower than the average RMSEV values of the FWC but with higher $R^2$ values than other wavelengths. Figure 4 shows the calculated baseline RMSEV values (black dashes, 12.4) for the FWC of the mixture samples. An EW region (475 to 775 nm) was then selected.

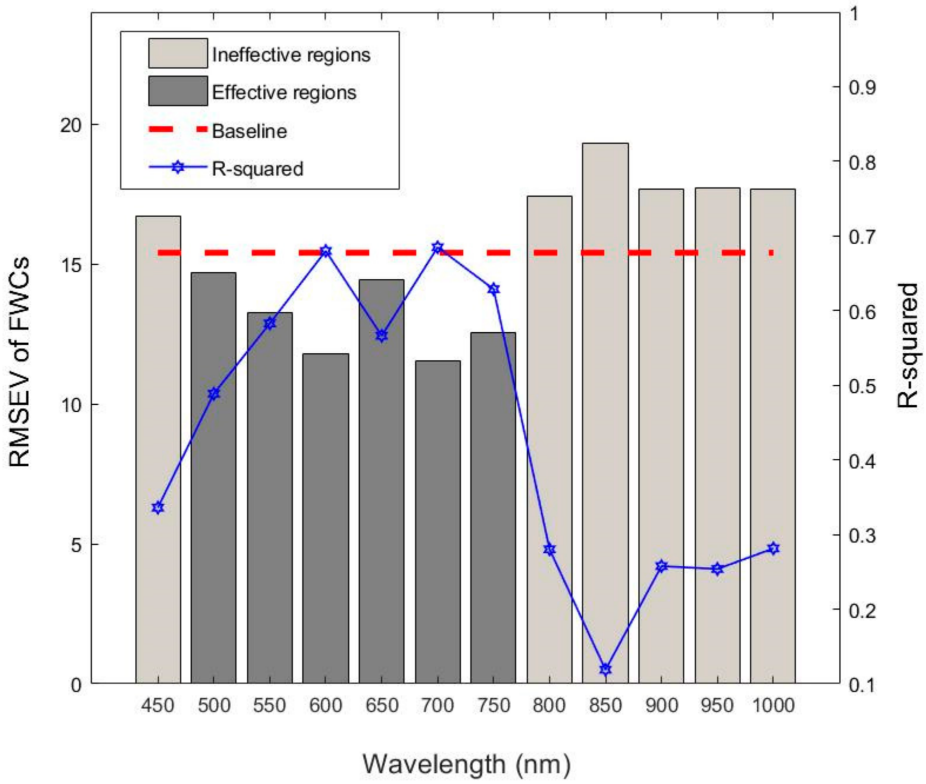


**Figure 4.** Selected effective wavelength region using FWC RMSEVs.

The beta coefficients of the developed PLS model are shown in Figure 5. Because the high peaks of the absolute values mainly influenced the model development, four wavelengths (470, 625, and 675 nm) were selected.

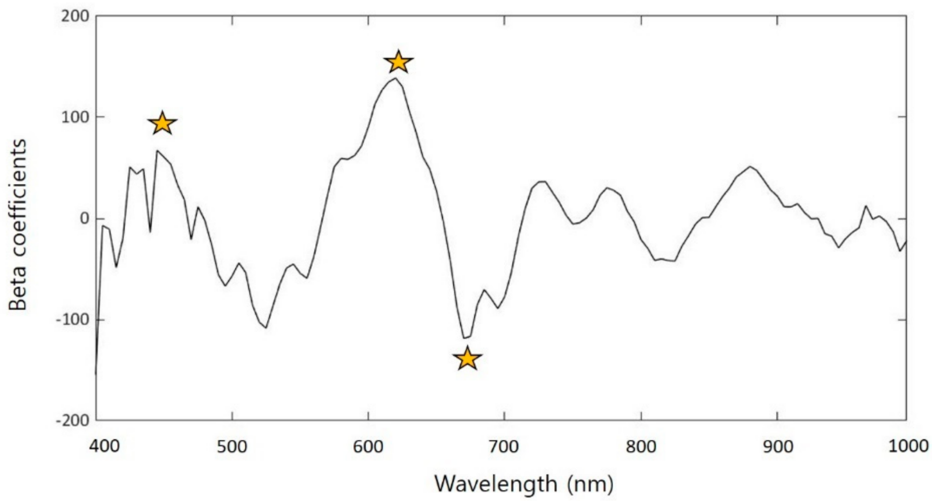


**Figure 5.** PLS model beta-coefficient plot for FWC detection in OF mixture samples.

Table 2 lists the results of both the PLS and LS-SVM models produced using five preprocessing methods within the selected EW region. The overall results of the LS-SVM model were superior to those of the PLS model. Based on $R^2$, SEC, and SEP, the LS-SVM model was selected. The correlations between the FWC concentrations, given by the mixture sample and by the LS-SVM model with the range normalization method, are shown in Figure 6.

**Table 2.** FWC prediction outcome for OF mixture samples from EW region.

| Models | Preprocessing | | Calibration $R_c^2$ | Calibration SEC (%) | Calibration Factors | Calibration Bias | Prediction $R_p^2$ | Prediction SEP (%) | Prediction Bias |
|---|---|---|---|---|---|---|---|---|---|
| PLS | Smoothing | | 0.74 | 10.35 | 9 | 0.69 | 0.65 | 12.27 | 0.57 |
| | Normalization | Mean | 0.79 | 9.47 | 6 | 0.74 | 0.76 | 10.12 | 0.10 |
| | | Maximum | 0.8 | 9.22 | 8 | 0.76 | 0.71 | 11.28 | 0.78 |
| | | Range | 0.77 | 9.73 | 8 | 0.73 | 0.68 | 11.7 | 0.76 |
| | MSC | | 0.77 | 9.77 | 7 | 0.73 | 0.67 | 12.03 | 5.03 |
| | SNV | | 0.75 | 10.18 | 7 | 0.71 | 0.69 | 11.53 | 0.53 |
| | SGD | 1st deri. | 0.75 | 10.28 | 7 | 0.68 | 0.66 | 11.94 | −0.12 |
| | | 2nd deri. | 0.79 | 9.32 | 9 | 0.67 | 0.68 | 11.68 | −0.06 |
| | Raw | | 0.73 | 10.52 | 8 | 0.69 | 0.676 | 11.73 | −0.20 |
| LS-SVM | Smoothing | | 0.9 | 6.44 | - | 0.76 | 0.76 | 10.03 | −0.12 |
| | Normalization | Mean | 0.85 | 7.86 | - | 0.82 | 0.82 | 8.62 | 1.17 |
| | | Maximum | 0.89 | 6.81 | - | 0.81 | 0.82 | 8.74 | 0.40 |
| | | Range | 0.87 | 7.44 | - | 0.83 | 0.83 | 8.46 | 0.94 |
| | MSC | | 0.9 | 6.36 | - | 0.83 | 0.83 | 8.55 | 4.53 |
| | SNV | | 0.92 | 5.85 | - | 0.81 | 0.81 | 8.96 | 0.78 |
| | SGD | 1st deri. | 0.95 | 4.5 | - | 0.83 | 0.84 | 8.34 | −0.36 |
| | | 2nd deri. | 0.99 | 2.26 | - | 0.78 | 0.78 | 9.64 | −0.24 |
| | Raw | | 0.89 | 6.75 | - | 0.83 | 0.83 | 8.52 | 0.41 |

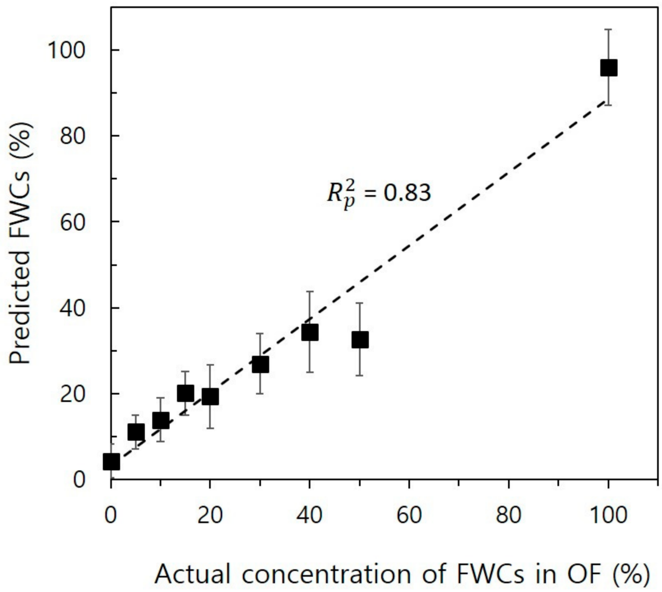


**Figure 6.** Correlation between actual and predicted FWC concentrations in mixture samples (0, 5, 10, 15, 20, 30, 40, 50, and 100%), for LS-SVM model with range normalization method.

### *3.3. FWC Visucalization in Mixture Samples*

Figure 7 shows representative images for increasing FWC content (0, 5, 10, 15, 20, 30, 40, 50, and 100%) in the mixture samples, which were obtained through application of the developed LS-SVM model to produce a distribution map of the FWCs of the mixture samples. Each LS-SVM image is 500 × 500 pixels in size. With increasing FWC, more pixels gradually change from blue to red; the color change index is described in the color bar.

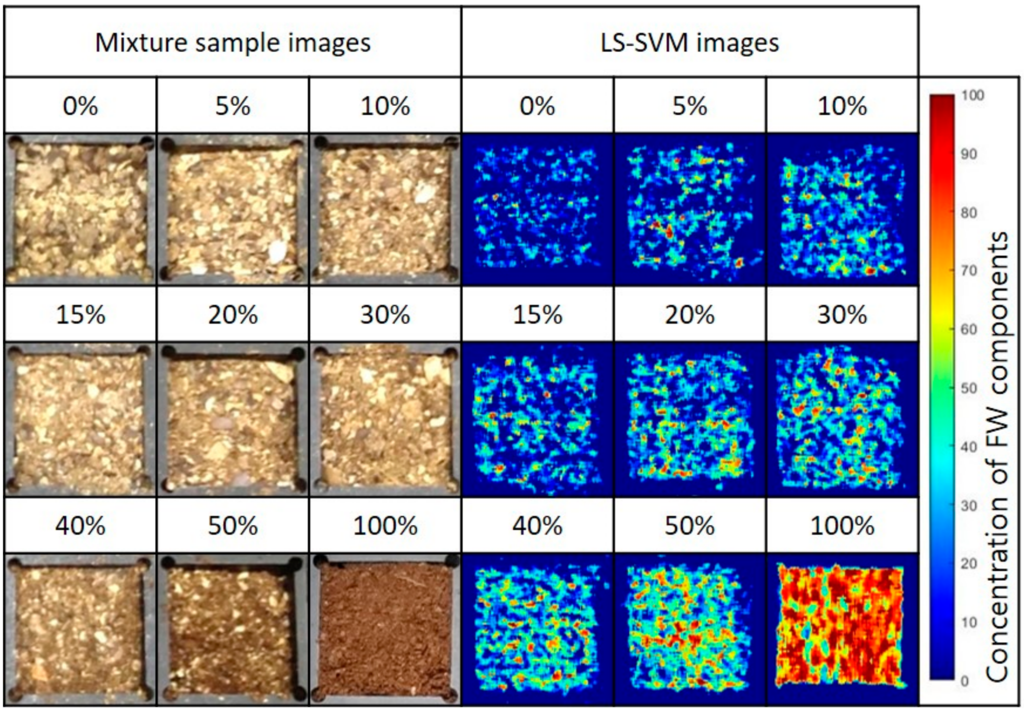


**Figure 7.** FWC visualization in mixture samples and images produced by LS-SVM model.

## 4. Discussion

### 4.1. Spectral Analysis

Vis/NIR region contains meaningful information about the major X–H chemical bonds, i.e., C–H, N–H and O–H. All of the molecules including hydrogen have a measurable Vis/NIR spectrum, resulting in a large amount of organic materials to be suitable for Vis/NIR analysis [34]. In Figure 3, the reflective spectral signatures of the mixture samples provide typical chemical information about the OF because they include overtones of the fundamental vibrations of the organic molecules and combination bands caused by the stretching and bending of N–H, C–H, and C–O groups, which primarily occur in the Vis/NIR region [35–37]. In particular, the spectral absorption region at 655 nm shows lipid component vibration. The feature waveband within the ranges of 600 to 700 nm is mainly assigned to the functional lipid groups including C–H, $CH_2$, and $CH_3$ bonds [38]. To produce FW fertilizer, oil waste is extracted and removed from FW through oil–water separation. After this separation process, the FW could be converted into biogas, for combined heat and power generation, or for fuel after purification. The remaining solid digestate was converted into OF and compost [11]. Despite the oil waste extraction process, however, some lipid components remained and were detected in the OF spectral absorption peak at 655 nm.

### 4.2. PLS and SVM Model Analysis

The RMSEV wavelength ranges smaller than the average RMSEV value in Figure 4 were used to identify EW regions for FWC in the mixture samples, while wavelengths with RMSEV values less than the average RMSEV value were considered to be unnecessary. Thus, only 50% of the entire spectrum included meaningful FWC spectral features and could be used for FWC prediction in the mixture samples.

In Figure 3, the lipid component affected the LS-SVM model in the 600- to 700-nm region; this feature is also apparent for the PLS beta coefficients. That is, in Figure 5, all wavelengths except those in the 600- to 700-nm region almost evenly affected the performance of the developed PLS model; therefore, this region would have a relatively large impact on the PLS model performance.

In Table 2, among the preprocessing methods, the range normalization method was selected as the optimal. This approach did not produce the highest coefficient of determination values for calibration and prediction ($R_c^2$ = 0.87 and $R_p^2$ = 0.83, respectively) or the lowest SEC (7.44%) and SEP (8.46%) values compared with the SGD method ($R_c^2$ = 0.99, $R_p^2$ = 0.83, SEC = 2.26%, and SEP = 8.34%), the balance of the two coefficients of determination exceeded that of the SGD method because the ideal ratio of calculation to prediction values is 1 [33] for optimal model selection.

The $R_p^2$ of 0.83 obtained in this work is lower than those of the authors' previous studies based on HSI techniques for foreign particle detection in powder materials [22] and food deterioration evaluation [27,32,33]. This low coefficient of determination may have been caused by the relationship between the particle size and the wavelength of the illumination employed in this work.

The disadvantage of the HSI technique is its low penetration depth, which occurs because of the scattering effects of photons on the specimen surface. In general, the average penetration depth depends on the imaging wavelength; the longer the wave, the deeper the penetration [39]. The penetration depth of Vis/NIR sensing is typically less than a millimeter [40], and the Vis/NIR region of this study was selected because of its color pigment selectivity for FWC detection. However, although the mixture samples containing FW particles used for this experiment were well-mixed, the FW particles may have been located toward the bottom or middle of the sample holders (3 mm). Thus, the model accuracy may have been affected by the FW particle positions. In future work, FWC particle sizes, according to penetration depth, will be investigated with application of different models in order to develop more precise prediction systems.

In powdered materials, the detection performance tends to decrease simultaneously with the target particle size [41]. The FWC particle sizes of this work were tens to hundreds of micrometers, whereas the other OF particle sizes ranged from 5 to 0.1 mm. Therefore, the model prediction accuracy gradually decreased with increased FWC concentration in the mixture samples, as shown in Figure 6. To improve the model performance, the sample holder height and the particle size should be controlled according to the light source and target particle size.

### 4.3. Ananlysis of Hyperspectral FWC Imaging

Although conventional spectroscopy techniques provide only one set of spectral information per individual sample, the HSI technique can produce full spectral information from every pixel. Thus, the mixture-sample images obtained using the LS-SVM model can show different spectral and spatial information for each pixel. In Figure 7, the mixture samples with different FWC levels are not easily distinguished by the naked eye, except for the 100% FWC sample. However, the LS-SVM images clearly classify the different FWC contents based on the number of yellow and red pixels, which increase with increasing FWC levels. Therefore, the obtained images present the FWC concentrations on a linear color scale with different colors being used for each pixel, facilitating improved understanding of the spatial variation in FWC content in the mixture samples.

From Figure 7, it is particularly difficult to evaluate the FWCs added to the OF up to 30% concentration with the naked eye. However, the LS-SVM approach detects and distinguishes the increasing concentrations. This is because the FW fertilizer has a different pigment to the other OF ingredients, as shown in Figure 7, and thus, the color difference between the two groups reveals the FWC level. Note that pigment-based spectral features could strongly affect the performance of the LS-SVM model and, thus, the output images. Consequently, application of chemometric methods with various preprocessing techniques, and the HSI technique used in this study has considerable potential for quantitative evaluation of FWCs in OF.

## 5. Conclusions

An HSI technique for the quantitative evaluation of FWCs in OF within the Vis/NIR region was investigated; the HSI system, image processing method, chemometrics models, and model preprocessing methods were developed and analyzed. The reflectance spectra in the Vis/NIR region, which were extracted from the hyperspectral images of mixture samples, were processed into the EW region (500 to 750 nm) for LS-SVM and PLS models. In the EW region, the spectral band of the lipid components between 600 and 700 nm mainly affects the hyperspectral images for determination of the FWCs in OF. After preprocessing was applied to both models, the LS-SVM model with range normalization was selected because of the stable performance of the coefficients of determination and the low SEP and SEC values. The $R_p^2$ obtained for evaluation of different FWC levels (0, 5, 10, 15, 20, 30, 40, 50, and 100%) was approximately 0.83 because of the different particle sizes in the mixture samples. However, the dynamic changes in the FWCs with increased concentration were clearly distinguished using distribution maps visualized using the LS-SVM model. Hence, the developed HSI technique may constitute an alternative method for a rapid and accurate inspection system for real-time quality screening to prevent excessive addition of FW fertilizer to OF. This approach introduces a promising research avenue for development of various nondestructive quality and safety evaluation systems for particle-based fertilizers.

**Author Contributions:** Conceptualization, H.L. and B.-K.C.; methodology, H.L. and B.-K.C.; software, H.L. and I.B.; validation, H.L. and G.K.; formal analysis, H.L. and G.K.; investigation, H.L., I.B. and G.K.; resources, H.L. and B.-K.C.; data curation, H.L. and G.K.; writing—original draft preparation, H.L. and G.K.; writing—review and editing, H.L., G.K., B.-K.C. and M.S.K. All authors have read and agreed to the published version of the manuscript.

**Funding:** This work was supported by Korea Institute of Planning and Evaluation for Technology in Food, Agriculture and Forestry (IPET) through Agri-Bio industry Technology Development Program, funded by Ministry of Agriculture, Food and Rural Affairs (MAFRA) (319114-3).

**Institutional Review Board Statement:** Not applicable.

**Informed Consent Statement:** Not applicable.

**Data Availability Statement:** Data available in a publicly accessible repository.

**Conflicts of Interest:** The authors declare no conflict of interest.

## References

1. Capson-Tojo, G.; Rouez, M.; Crest, M.; Steyer, J.P.; Delgenès, J.P.; Escudié, R. Food waste valorization via anaerobic processes: A review. *Rev. Environ. Sci. Biotechnol.* **2016**, *15*, 499–547. [CrossRef]
2. Chiew, Y.L.; Spångberg, J.; Baky, A.; Hansson, P.A.; Jönsson, H. Environmental impact of recycling digested food waste as a fertilizer in agriculture—A case study. *Resour. Conserv. Recycl.* **2015**, *95*, 1–14. [CrossRef]
3. Kim, M.H.; Kim, J.W. Comparison through a LCA evaluation analysis of food waste disposal options from the perspective of global warming and resource recovery. *Sci. Total Environ.* **2010**, *408*, 3998–4006. [CrossRef]
4. Vaverková, M.D.; Adamcová, D.; Winkler, J.; Koda, E.; Červenková, J.; Podlasek, A. Influence of a municipal solid waste landfill on the surrounding environment: Landfill vegetation as a potential risk of allergenic pollen. *Int. J. Environ. Res. Public Health* **2019**, *16*, 64. [CrossRef]
5. Palmiotto, M.; Fattore, E.; Paiano, V.; Celeste, G.; Colombo, A.; Davoli, E. Influence of a municipal solid waste landfill in the surrounding environment: Toxicological risk and odor nuisance effects. *Environ. Int.* **2014**, *68*, 16–24. [CrossRef] [PubMed]
6. Thassitou, P.K.; Arvanitoyannis, I.S. Bioremediation: A novel approach to food waste management. *Trends Food Sci. Technol.* **2001**, *12*, 185–196. [CrossRef]
7. Stabnikova, O.; Ding, H.B.; Tay, J.H.; Wang, J.Y. Biotechnology for aerobic conversion of food waste into organic fertilizer. *Waste Manag. Res.* **2005**, *23*, 39–47. [CrossRef] [PubMed]
8. Hamid, H.A.; Harun, H.; Sunar, N.; Muhammad, M.S.; Hamidon, N.; Ali, R.; Ahmad, F.H.; Qi, L.P. Development of Organic Fertilizer From Food Waste By Composting in Uthm Pagoh. *Sustain. Environ. Technol.* **2018**, *1*, 1–6.
9. Acosta-Motos, J.R.; Ortuño, M.F.; Bernal-Vicente, A.; Diaz-Vivancos, P.; Sanchez-Blanco, M.J.; Hernandez, J.A. Plant responses to salt stress: Adaptive mechanisms. *Agronomy* **2017**, *7*, 18. [CrossRef]
10. Lee, I.B.; Kim, P.J.; Chang, K.W. Evaluation of stability of compost prepared with korean food wastes. *Soil Sci. Plant Nutr.* **2002**, *48*, 1–8. [CrossRef]

11. Jin, C.; Sun, S.; Yang, D.; Sheng, W.; Ma, Y.; He, W.; Li, G. Anaerobic digestion: An alternative resource treatment option for food waste in China. *Sci. Total Environ.* **2021**, *779*, 146397. [CrossRef]
12. Kim, Y.; Kim, D.; Lee, G. Physicochemical Properties of a Mixture of Dried Food Waste Powder with Organic Fertilizer and Effects on the Growth of Major Leafy Vegetable. *J. Korea Org. Resour. Recycl. Assoc.* **2019**, *27*, 5–13. [CrossRef]
13. Amanah, H.Z.; Joshi, R.; Masithoh, R.E.; Choung, M.-G.; Kim, K.-H.; Kim, G.; Cho, B.-K. Nondestructive measurement of anthocyanin in intact soybean seed using Fourier Transform Near-Infrared (FT-NIR) and Fourier Transform Infrared (FT-IR) spectroscopy. *Infrared Phys. Technol.* **2020**, *111*, 103477. [CrossRef]
14. Kim, G.; Baek, I.; Stocker, M.D.; Smith, J.E.; Van Tassell, A.L.; Qin, J.; Chan, D.E.; Pachepsky, Y.; Kim, M.S. Hyperspectral Imaging from a Multipurpose Floating Platform to Estimate Chlorophyll-a Concentrations in Irrigation Pond Water. *Remote Sens.* **2020**, *12*, 2070. [CrossRef]
15. Kim, M.S.; Chen, Y.R.; Mehl, P.M. Hyperspectral reflectance and fluorescence imaging system for food quality and safety. *Trans. ASAE* **2001**, *44*. [CrossRef]
16. An, D.; Zhao, G.; Chang, C.; Wang, Z.; Li, P.; Zhang, T.; Jia, J. Hyperspectral field estimation and remote-sensing inversion of salt content in coastal saline soils of the Yellow River Delta. *Int. J. Remote Sens.* **2016**, *37*, 455–470. [CrossRef]
17. Kumar, J.P.; Deshpande, S.; Inamdar, A. Detection of Fertilizer Quantity in Soil Using Hyperspectral Data. In Proceedings of the 9th Workshop on Hyperspectral Image and Signal Processing: Evolution in Remote Sensing, Amsterdam, The Netherlands, 1–4 September 2018. [CrossRef]
18. Wang, Y.; Hu, X.; Hou, Z.; Ning, J.; Zhang, Z. Discrimination of nitrogen fertilizer levels of tea plant (*Camellia sinensis*) based on hyperspectral imaging. *J. Sci. Food Agric.* **2018**, *98*, 4659–4664. [CrossRef] [PubMed]
19. Sha, W.; Li, J.; Xiao, W.; Ling, P.; Lu, C. Quantitative analysis of elements in fertilizer using laser-induced breakdown spectroscopy coupled with support vector regression model. *Sensors* **2019**, *19*, 3277. [CrossRef]
20. Lin, Z.; Wang, R.; Wang, Y.; Wang, L.; Lu, C.; Liu, Y.; Zhang, Z.; Zhu, L. Accurate and rapid detection of soil and fertilizer properties based on visible/near-infrared spectroscopy. *Appl. Opt.* **2018**, *57*, D69. [CrossRef] [PubMed]
21. Kira, O.; Linker, R.; Gitelson, A. Non-destructive estimation of foliar chlorophyll and carotenoid contents: Focus on informative spectral bands. *Int. J. Appl. Earth Obs. Geoinf.* **2015**, *38*, 251–260. [CrossRef]
22. Lee, H.; Kim, M.S.; Lohumi, S.; Cho, B.-K. Detection of melamine in milk powder using MCT-based short-wave infrared hyperspectral imaging system. *Food Addit. Contam. Part A* **2018**, *35*, 1027–1037. [CrossRef] [PubMed]
23. Yi, Q.; Jiapaer, G.; Chen, J.; Bao, A.; Wang, F. Different units of measurement of carotenoids estimation in cotton using hyperspectral indices and partial least square regression. *ISPRS J. Photogramm. Remote Sens.* **2014**, *91*, 72–84. [CrossRef]
24. Yuan, H.; Yang, G.; Li, C.; Wang, Y.; Liu, J.; Yu, H.; Feng, H.; Xu, B.; Zhao, X.; Yang, X. Retrieving soybean leaf area index from unmanned aerial vehicle hyperspectral remote sensing: Analysis of RF, ANN, and SVM regression models. *Remote Sens.* **2017**, *9*, 309. [CrossRef]
25. Lante, A.; Lomolino, G.; Cagnin, M.; Spettoli, P. Content and characterisation of minerals in milk and in Crescenza and Squacquerone Italian fresh cheeses by ICP-OES. *Food Control* **2006**, *17*, 229–233. [CrossRef]
26. Li, W.; Simmons, P.; Shrader, D.; Herrman, T.J.; Dai, S.Y. Microwave plasma-atomic emission spectroscopy as a tool for the determination of copper, iron, manganese and zinc in animal feed and fertilizer. *Talanta* **2013**, *112*, 43–48. [CrossRef]
27. Baek, I.; Lee, H.; Cho, B.; Mo, C.; Chan, D.E.; Kim, M.S. Shortwave infrared hyperspectral imaging system coupled with multivariable method for TVB-N measurement in pork. *Food Control* **2021**, *124*, 107854. [CrossRef]
28. Faqeerzada, M.A.; Perez, M.; Lohumi, S.; Lee, H.; Kim, G.; Wakholi, C.; Joshi, R.; Cho, B.-K. Online Application of a Hyperspectral Imaging System for the Sorting of Adulterated Almonds. *Appl. Sci.* **2020**, *10*, 6569. [CrossRef]
29. Faqeerzada, M.A.; Lohumi, S.; Kim, G.; Joshi, R.; Lee, H.; Kim, M.S.; Cho, B.-K. Hyperspectral Shortwave Infrared Image Analysis for Detection of Adulterants in Almond Powder with One-Class Classification Method. *Sensors* **2020**, *20*, 5855. [CrossRef]
30. Qin, J.; Chao, K.; Kim, M.S.; Lu, R.; Burks, T.F. Hyperspectral and multispectral imaging for evaluating food safety and quality. *J. Food Eng.* **2013**, *118*, 157–171. [CrossRef]
31. Christopher, J.C. Burgers A Tutorial on Support Vector Machines for Pattern Recognition. *Data Min. Knowl. Discov.* **1998**, *2*, 121–167.
32. Lee, H.; Kim, M.S.; Lee, W.H.; Cho, B.K. Determination of the total volatile basic nitrogen (TVB-N) content in pork meat using hyperspectral fluorescence imaging. *Sens. Actuators B Chem.* **2018**, *259*, 532–539. [CrossRef]
33. Lee, H.; Cho, B.-K.; Kim, M.S.; Lee, W.-H.; Tewari, J.; Bae, H.; Sohn, S.-I.; Chi, H.-Y. Prediction of crude protein and oil content of soybeans using Raman spectroscopy. *Sensors Actuators B Chem.* **2013**, *185*, 694–700. [CrossRef]
34. Manley, M. Near-infrared spectroscopy and hyperspectral imaging: Non-destructive analysis of biological materials. *Chem. Soc. Rev.* **2014**, *43*, 8200–8214. [CrossRef] [PubMed]
35. Ilani, T.; Herrmann, I.; Karnieli, A.; Arye, G. Characterization of the biosolids composting process by hyperspectral analysis. *Waste Manag.* **2016**, *48*, 106–114. [CrossRef]
36. Ben-Dor, E.; Inbar, Y.; Chen, Y. The reflectance spectra of organic matter in the visible near-infrared and short wave infrared region (400–2500 nm) during a controlled decomposition process. *Remote Sens. Environ.* **1997**, *61*, 1–15. [CrossRef]
37. Curran, P.J. Remote sensing of foliar chemistry. *Remote Sens. Environ.* **1989**, *30*, 271–278. [CrossRef]
38. Chu, B.; Chen, K.; Pan, X.; Wu, Q.; Liu, S.; Gong, J.; Li, X. Visible/Short-wave near-infrared hyperspectral analysis of lipid concentration and fatty acid unsaturation of Scenedesmus obliquus in situ. *Comput. Electron. Agric.* **2021**, *182*, 106046. [CrossRef]

39. Clarke, F.C.; Hammond, S.V.; Jee, R.D.; Moffat, A.C. Determination of the information depth and sample size for the analysis of pharmaceutical materials using reflectance near-infrared microscopy. *Appl. Spectrosc.* **2002**, *56*, 1475–1483. [CrossRef]
40. Baveye, P.C.; Laba, M. Visible and near-infrared reflectance spectroscopy is of limited practical use to monitor soil contamination by heavy metals. *J. Hazard. Mater.* **2015**, *285*, 137–139. [CrossRef]
41. Fu, X.; Chen, J.; Zhang, J.; Fu, F.; Wu, C. Effect of penetration depth and particle size on detection of wheat flour adulterant using hyperspectral imaging. *Biosyst. Eng.* **2021**, *204*, 64–78. [CrossRef]